PCCP

PAPER

View Article Online
View Journal | View Issue

Cite this: *Phys. Chem. Chem. Phys.*, 2014, **16**, 14161

IRMPD spectroscopy of metalated flavins: structure and bonding of M^{q+}–lumichrome complexes (M^{q+} = Li^+–Cs^+, Ag^+, Mg^{2+})†

Alan Günther,[a] Pablo Nieto,[a] Giel Berden,[b] Jos Oomens[bc] and Otto Dopfer*[a]

Received 8th April 2014,
Accepted 25th May 2014

DOI: 10.1039/c4cp01524j

www.rsc.org/pccp

Infrared multiphoton dissociation (IRMPD) spectra of mass selected isolated metal–lumichrome ionic complexes, $M^{q+}LC_n$ with M^{q+} = Li^+, Na^+, K^+, Rb^+, Cs^+, Ag^+ (n = 1), and Mg^{2+} (n = 2), are recorded in the fingerprint range. The complexes are generated in an electrospray ionization source coupled to an ion cyclotron mass spectrometer and the IR free electron laser FELIX. Vibrational and isomer assignments of the IRMPD spectra are accomplished by density functional theory calculations at the B3LYP/cc-pVDZ level, which provide insight into the structure, binding energy, bonding mechanism, and spectral properties of the complexes. The two major binding sites identified involve metal bonding to the oxygen atoms of the two available carbonyl groups of LC (denoted O2 and O4). The more stable O4 isomer benefits from an additional interaction with the lone pair of the nearby N5 atom of LC. While M^+LC with alkali metals are mainly stabilized by electrostatic forces, the Ag^+LC complex reveals additional stabilization arising from partly covalent contributions. Finally, the interaction of Mg^{2+} ions with LC is largely enhanced by the doubled positive charge. The frequencies of the C=O stretching modes are a sensitive indicator of both the metal binding site and the metal bond strength.

1. Introduction

Flavins are a fundamental class of bioorganic molecules. They are derived from a 7,8-dimethyl-10-alkylisoalloxazine chromophore also known as lumichrome (LC, Fig. 1). Their diverse properties make flavins of paramount importance for many biological systems.[1–6] For instance, flavins absorb in a wide spectral range from the optical up to the UV region, and their absorption maxima vary sensitively with structural modifications. In this way, flavin-containing domains act as light-harvesting modules in plants and algal phototropins and as blue-light receptors in fungals.[5] Furthermore, as an important component of flavoproteins they are involved in the repair of DNA,[7] serve as cofactor in the enzyme GOx which oxidizes glucose to hydrogen peroxide, and are involved in the redox cycle of the respiratory chain by acting as an electron donor and acceptor.[6] Their broad (bio-)chemical activity is based on the existence of three different oxidation states, namely, the oxidized state (flavoquinone), the singly reduced or radical state

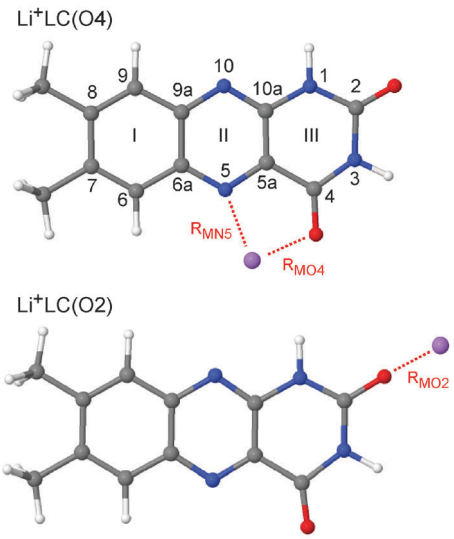

Fig. 1 Structures of the planar O4 and O2 isomers of M^+LC illustrated for M = Li, including the atomic and ring numbering (according to IUPAC).

[a] *Institut für Optik und Atomare Physik, Technische Universität Berlin, Hardenbergstr. 36, D-10623 Berlin, Germany. E-mail: dopfer@physik.tu-berlin.de; Fax: +49 30 314 23018*
[b] *Institute for Molecules and Materials, FELIX facility, Radboud University Nijmegen, Toernooiveld 7, 6525 ED Nijmegen, The Netherlands*
[c] *van't Hoff Institute for Molecular Sciences, University of Amsterdam, Science Park 904, 1098XH Amsterdam, The Netherlands*

† Electronic supplementary information (ESI) available: (1) Laser power dependence; (2) IR spectra of Li^+LC(O4) at different theoretical levels; (3) IRMPD spectrum of Li^+LC compared to IR spectra calculated for different isomers; (4–6) properties of $M^{q+}LC_n$ as a function of $1/R_M$; (7) IRMPD spectrum of Li^+LC compared to IR spectra calculated for Li^+iso-LC isomers; (8) IRMPD spectra of Li^+LC and Ag^+LC compared to calculated spectra; (9) NBO charges of LC. See DOI: 10.1039/c4cp01524j

(flavosemiquinone), and the fully reduced state (flavohydroquinone). Flavins are able to photooxidize metal ions such as Fe(II) and catalyze the photoreduction of Fe(III).[8] Thus, some bacteria are capable to catalyze redox reactions, *e.g.* of insoluble Fe(III) oxide minerals with different electrodes, in which flavins, most notably riboflavin, play a decisive role.[9] The interaction of (alkali) metal ions with lumichrome (LC) forming a metal flavoquinone chelate, the smallest member of the flavins, can serve as a benchmark system for elucidating such processes at the molecular level. Such metal chelates are transient species in aqueous solution.

Various properties of metal–flavin complexes were extensively investigated in solution.[8,10–15] Here, the complexation with metals has an important influence on the electronic and redox properties of the flavin, which is signalled by large shifts in the absorption spectra.[11] However, the considerable influence of the solvent and counter ions in these studies is not well characterized. Thus, spectroscopic studies on isolated molecules and their aggregates are required to provide information about the structural, electronic, and chemical properties of the bare optically active substance. Basic properties of flavins, their ground-state structure, their stability, and their interaction with metal ions and solvent must be characterized to generate a consistent molecular-level description of their activity and function.[16] However, due to their difficult preparation in the gas phase, experiments on isolated flavins have not been performed until recently,[17–19] and studies of their metal and solvent adducts are completely lacking. The few available studies include photo- and collision-induced fragmentation of protonated flavin mononucleotide (FMN),[19] a fluorescence spectrum of lumichrome (LC) in superfluid He droplets,[20] and the determination of the proton affinity of lumiflavin (LF) by mass spectrometry.[17] Moreover, the preferred protonation site of a variety of fundamental protonated flavins, including LC, LF, riboflavin (RF, vitamin B_2), and FMN, have recently been determined by infrared multiphoton dissociation (IRMPD) spectroscopy and quantum chemical calculations.[18] It was shown that the protonation site strongly depends on the flavin substituent and that the strongly IR active CO stretch modes are sensitive indicators of the various protonation sites.[18] In the present investigation, we extend these IRMPD studies to metalated flavins, namely M^{q+}LC with the closed-shell metal ions, M^{q+} = Li^+, Na^+, K^+, Rb^+, Cs^+, Ag^+, and Mg^{2+}, using the same experimental and computational strategy. Systematic analysis of M^+LC within the series of the alkali ions reveals the effects of the size of the metal ion on the preferred binding site, the metal binding energy, and the bonding mechanism. Comparison with Ag^+LC focuses on possible additional contributions of covalent bonding arising from its nature as a transition metal. The Mg^{2+} ion has been chosen to study the effect of the charge on the M^{q+}LC interaction. Since flavins are chromophores, which have been analyzed in solution extensively, it is of interest to explore the influence of an additional charge of the metal ion on their optical properties. In flavins, optical excitation is primarily provided by n → π* and π → π* transitions.[2] Metal cations bind to the aromatic chromophore *via* π stacking or to nucleophilic N and O centers *via* σ bonding, and thus may substantially modify the electronic structure of both the π and n orbitals, which in turn change the photochemistry of the LC chromophore.

Here, the M^{q+}LC complexes are transferred into the gas phase by electrospray ionization, and their IR spectra recorded by infrared multiple-photon dissociation (IRMPD) in a Fourier-Transform Ion Cyclotron Resonance Mass Spectrometer (FT-ICR-MS) are analyzed by density functional calculations to obtain a deeper understanding of their properties. This combined strategy has proven to be a powerful tool to characterize metal ion complexes of a large variety of (bio-)molecules.[21–33] Similar to protonated flavins,[18] the CO stretch modes serve as the main indicator of the metal binding sites. The comparison of the measured IRMPD spectra with the calculated linear absorption spectra provides insight into their respective structures and bonding mechanisms.

2. Experimental and computational techniques

The IRMPD spectra of $M^{q+}LC_n$ complexes with M^{q+} = Li^+, Na^+, K^+, Rb^+, Cs^+, and Ag^+ (n = 1) and Mg^{2+} (n = 2) shown in Fig. 2 are recorded in the fingerprint range in a FT-ICR-MS coupled to an ESI ion source and the IR beamline of the Free Electron Laser for Infrared eXperiments (FELIX).[34–36] LC (>99%) purchased from Sigma Aldrich is used without further purification. To produce the metal complexes, a 0.2 mM solution of LC in methanol is mixed with 1–6 mM metal chloride or nitrate salt solutions in water. In the case of Ag^+ and Mg^{2+}, acetonitrile is used as solvent instead of water. In contrast to Ag^+LC, all efforts

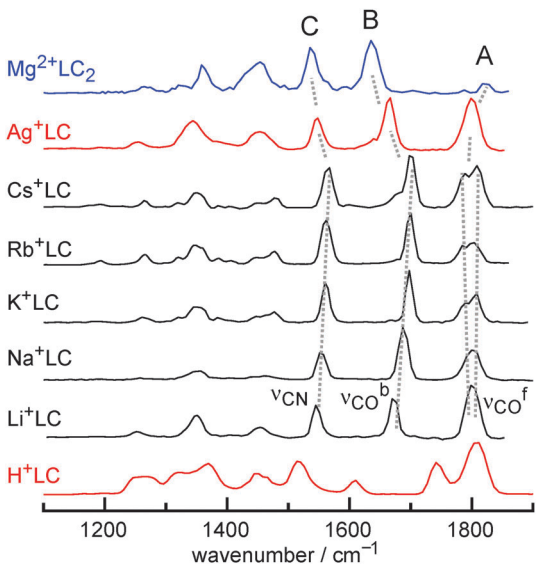

Fig. 2 IRMPD spectra of $M^{q+}LC_n$ recorded in the fingerprint range compared to corresponding spectrum of H^+LC.[18] Corresponding transitions assigned to the free and bound C=O stretch modes (A, B) and the intense ring C–N/C–C stretch mode (C) are connected by dotted lines and listed in Table 1. The relative intensity of band A in the $Mg^{2+}LC_2$ spectrum is reduced due to reduced laser power in this frequency range.

to generate Cu^+LC or Au^+LC in the ESI source failed in solvents like methanol, acetonitrile and mixtures with formic acid. The solutions are sprayed at a flow rate of 10 μl min^{-1}. The generated ions are accumulated in a hexapole ion trap and transferred *via* an octopole ion guide into the ICR cell. Here, the $M^{q+}LC_n$ complexes are mass selected and irradiated with 12 macropulses from FELIX operating at a repetition rate of 10 Hz. The typical macropulse energy is measured as 20–30 mJ in the range 700–1500 cm^{-1} and slowly degrades toward higher wavenumber. A plot of the frequency-dependent laser intensity is available in Fig. S1 in ESI.† The bandwidth of the FELIX radiation is specified as 0.5% FWHM of the central wavelength. Calibration of the wavelength with an accuracy of ±0.02 μm is achieved by a grating spectrometer. Depending on the scanned frequency range, the laser step size varies between 3 and 8 cm^{-1}. Parent and fragment ion intensities, I_P and I_F, are monitored as a function of the laser frequency, and the IRMPD yield is determined as $I_{IRMPD} = I_F/(I_P + I_F)$. For M^+LC, the monitored fragment ions are M^+ arising from loss of the neutral LC ligand. The doubly charged $Mg^{2+}LC_2$ complexes fragment into the two singly charged $[MgOH]^+LC$ and $[LC–OH]^+$ ions upon IRMPD. As the IR spectra are essentially the same for individual isotopes of M^{q+} at the current spectral resolution, they are averaged. The widths of individual transitions in the IRMPD spectra are of the order of 20 cm^{-1} and arise from a combination of the laser bandwidth, unresolved rotational structure, and the effects of the multiple-photonic character of the IRMPD process. The IRMPD yields are linearly normalized for variations in the laser intensity.

DFT calculations at the B3LYP/cc-pVDZ level are carried out for the different $M^{q+}LC_n$ complexes using GAUSSIAN09 and TURBOMOLE (version 6.5).[37,38] Relativistic corrections for the heavy metal cations (K^+, Rb^+, Cs^+, Ag^+) are included using the Stuttgart VDZ effective core potentials (ECP).[39] Calculated harmonic vibrational frequencies are empirically scaled by the factors 0.964 and 0.973 for the lighter (H, Li, Na, Mg) and heavier metal atoms, respectively (*vide infra*). All energies are corrected for zero point vibrational energies. In addition to binding energies (E), the Gibbs free energies (G) are evaluated at 298 K. At this stage, one should recall that IRMPD relies on multiple-photon absorption and subsequent dissociation, which may lead to modest redshifts and intensity modifications compared to a linear single-photon absorption spectrum.[36,40] The reliability of the computational approach is verified by calculating the IR spectra for a given isomer of Li^+LC at different levels of theory, including B3LYP/cc-pVDZ, B3LYP/cc-pVTZ, BP86/cc-pVTZ, MP2/cc-pVTZ (Fig. S2 in ESI†). This comparison reveals that the computationally economic B3LYP/cc-pVDZ results are similar to those at the higher levels. Furthermore, they reproduce semi-quantitatively the measured IRMPD spectrum with respect to both the frequencies and relative IR intensities. The charge distribution is evaluated using the Natural Bonding Orbital (NBO) analysis.

3. Results and discussion

Fig. 2 compares the IRMPD spectra recorded for all considered $M^{q+}LC_n$ complexes with that of H^+LC reported recently.[18] The results for the alkali ion–LC complexes will be discussed first, followed by those for Ag^+LC and $Mg^{2+}LC_2$.

3.1 M^+LC with M = Li–Cs

The IRMPD spectra of the M^+LC complexes with alkali ions in Fig. 2 exhibit three dominant peaks labelled A–C in the 1500–1850 cm^{-1} range. Although other less intense bands are resolved below 1500 cm^{-1}, the three bands assigned to the two C═O stretch modes (ν_{CO}, A–B) and one ring C–C/C–N stretch mode (ν_{CN}, C) characterize the isomers present in the experiments due to their high intensity and spectral variation and allow for the discrimination of different metal binding sites, as demonstrated previously for protonated flavins.[18] The positions of their maxima are summarized in Table 1, along with their vibrational and isomer assignment. Band A, located at 1799 cm^{-1} for Li^+LC, is split for the M^+LC complexes with the larger K^+, Rb^+ and Cs^+ ions. Bands B and C, located at 1670 and 1547 cm^{-1} for Li^+LC, shift to higher frequencies for heavier alkali atoms.

Several metal binding sites are considered for each M^+LC complex. The metal cation may bind to the nucleophilic sites of LC, such as the lone pairs of the oxygen atoms of the two C═O groups (denoted O2 and O4), the lone pairs of the two heterocyclic nitrogen atoms (N10 and N5), and π stacking to the aromatic rings (I–III). The calculations for Li^+LC reveal five different stable isomers with σ-bonding to O4, O2, and N10,

Table 1 Maxima (cm^{-1}) of the three bands A–C observed in the IRMPD spectra of a $M^{q+}LC_n$ (Fig. 2), along with their vibrational and isomer assignment

	Position	Assignment[a]
Li^+LC	1799 (A)	ν_{C2O} (O4 isomer)/ν_{C4O} (O2 isomer)
	1670 (B)	ν_{C4O} (O4 isomer)/ν_{C2O} (O2 isomer)
	1547 (C)	ν_{CN} (O4/O2 isomer)
Na^+LC	1799 (A)	ν_{C2O} (O4 isomer)/ν_{C4O} (O2 isomer)
	1688 (B)	ν_{C4O} (O4 isomer)/ν_{C2O} (O2 isomer)
	1554 (C)	ν_{CN} (O4/O2 isomer)
K^+LC	1808 (A)	ν_{C2O} (O4 isomer)
	1789 (A)	ν_{C4O} (O2 isomer)
	1698 (B)	ν_{C4O} (O4 isomer)/ν_{C2O} (O2 isomer)
	1561 (C)	ν_{CN} (O4/O2 isomer)
Rb^+LC	1804 (A)	ν_{C2O} (O4 isomer)
	1784 (A)	ν_{C4O} (O2 isomer)
	1700 (B)	ν_{C4O} (O4 isomer)/ν_{C2O} (O2 isomer)
	1562 (C)	ν_{CN} (O4/O2 isomer)
Cs^+LC	1808 (A)	ν_{C2O} (O4 isomer)
	1789 (A)	ν_{C4O} (O2 isomer)
	1700 (B)	ν_{C4O} (O4 isomer)/ν_{C2O} (O2 isomer)
	1565 (C)	ν_{CN} (O4/O2 isomer)
Ag^+LC	1799 (A)	ν_{C2O} (O4 isomer)
	1665 (B)	ν_{C4O} (O4 isomer)
	1548 (C)	ν_{CN} (O4 isomer)
$Mg^{2+}LC_2$	1822 (A)	ν_{C2O} (O4 isomer)
	1636 (B)	ν_{C4O} (O4 isomer)
	1538 (C)	ν_{CN} (O4 isomer)

[a] ν_{CN} is a coupled C–N/C–C stretch mode largely delocalized over the ring skeleton.

Table 2 Binding and relative (free) energies (kJ mol^{-1}) of $M^{q+}LC_n$(O4) and $M^{q+}LC_n$(O2) calculated at the B3LYP/cc-pVDZ level

	E(O4)	ΔE_{O4-O2}	G(O4)	ΔG_{O4-O2}
H^+LC^a	914.2	48.6	913.8	47.7
Li^+LC	304.0	71.5	272.3	67.9
Na^+LC	223.6	55.6	191.7	51.7
K^+LC	177.4	40.0	147.3	37.1
Rb^+LC	156.6	36.4	126.8	33.7
Cs^+Lc	140.3	31.5	111.4	29.1
Ag^+LC^b	294.2	92.9	260.5	86.1
$Mg^{2+}LC$	838.1	177.3	803.4	171.6
$Mg^{2+}LC_2$	1334.4	267.1	1250.9	256.2

[a] O4 is the O4+ structure and O2 is the O2− structure from ref. 18. [b] O2 is the O2− structure following the notation in ref. 18 (Fig. 4).

and π-stacking to the benzene (I) and pyrimidine (III) rings, with binding free energies of 272, 204, 133, 108, and 75 kJ mol^{-1}, respectively (Fig. S3 in ESI†). Clearly, the O4 and O2 isomers are by far the most stable ones, and indeed only these two isomers match the experimental results (Fig. S3 in ESI†). Significantly, the large splitting between the bands A and B assigned to free and bound C═O stretch modes (ν^f_{CO}, ν^b_{CO}), respectively, is indicative of metal bonding to one of the two available C═O groups and thus a clearcut signature for the presence of the O4 and/or O2 isomers. Thus, only those isomers will be considered further for the other M^+LC complexes (Na–Cs). Their calculated binding energies (E) and free energies (G) are listed in Table 2, and their calculated absorption spectra are compared in Fig. 3 to the IRMPD spectra. The spectra of bare LC and H^+LC[18] are also shown for comparison. The frequencies for LC, H^+LC, Li^+LC, and Na^+LC are scaled with 0.964, which matches band A of the Li^+LC spectrum to the C2O stretch frequency (ν_{C2O}) of Li^+LC(O4). The spectra of M^+LC with M = K–Cs are scaled with 0.973 resulting from fitting ν_{C2O} of K^+LC(O4) to the high-frequency component of the A doublet. The choice of two different scaling factors results from the two different computational approaches used for the lighter and heavier alkali ions (without and with effective core potential). The energetic, structural, and vibrational properties of the O4 and O2 isomers of $M^{q+}LC_n$ relevant for the present work are summarized in Tables 2–4 and visualized in Fig. S4–S6 in ESI† as a function of the inverse ionic radius of M^{q+}.

For all M^+LC complexes, the planar O4 isomer (C_s), in which M^+ binds in a chelate configuration to the lone pairs of both the O4 and N5 atoms, is the most stable structure (Fig. 1, Table 2). The binding energy of M^+LC(O4) decreases from 304 to 140 kJ mol^{-1} as the alkali metal ion increases from Li to Cs, and the free energies follow the same trend (272–111 kJ mol^{-1}, Fig. S4 in ESI†). The bond lengths of M^+ to the O4 and N5 atoms increase with the size of M^+ (R_{MO4} = 1.87–2.81 Å, R_{MN5} = 2.19–3.30), due to the increasing ionic radius (0.76–1.67 Å) and the decreasing interaction energy (Table 3, Fig. S5 in ESI†). The chelate angle α_{N5MO4} decreases from 89 to 54°, whereas at the same time the angle α_{MO4C4} opens up from 110 to 130°. The chelate is quite asymmetric, with shorter bonds to O4 and longer bonds to N5, and this asymmetry increases with increasing M^+ size, consistent with the M^+–O4 bond being stronger than the M^+–N5 bond. In the limit of vanishing interaction with

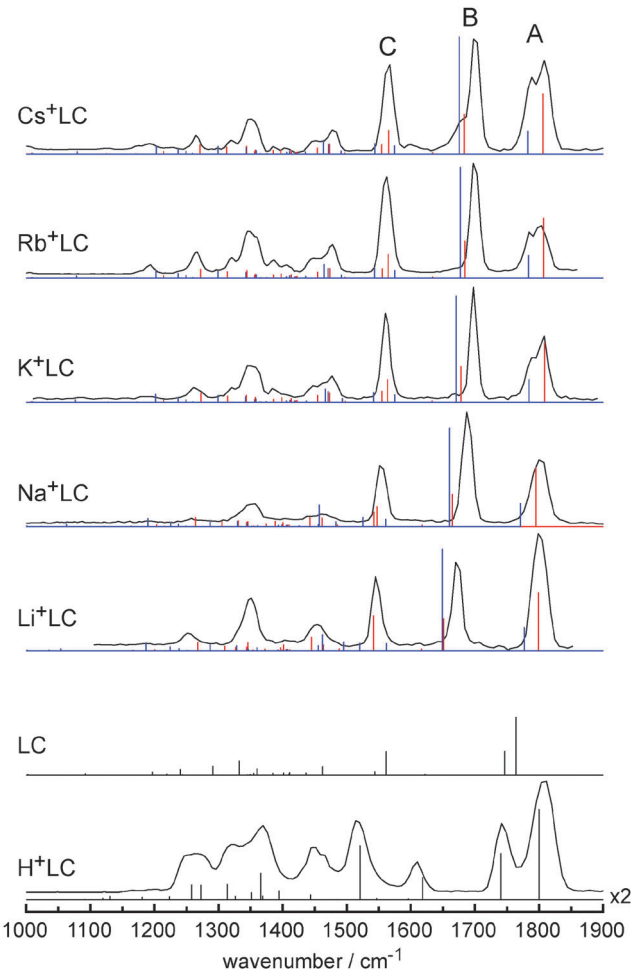

Fig. 3 IRMPD spectra of M^+LC with the alkali metals Li–Cs compared to linear IR stick absorption spectra of the O4 (red) and O2 (blue) isomers obtained at the B3LYP/cc-pVDZ level. The IRMPD spectrum of H^+LC[18] is also shown along with the spectrum calculated for the most stable N5 protonated isomer. For comparison, the IR spectrum calculated for LC is also shown.

N5, the C4–O4–M bonding would be roughly linear (as observed for the O2 isomers, *vide infra*). The interaction between the closed-shell alkali cations and LC is mostly based on electrostatic and induction forces, which in the long range are dominated by forces between the positive charge and the dipole and quadrupole moments of LC and its polarizability. As the ionization energy of LC (calculated as IE = 7.99 eV) is much higher than those of the alkali metals (IE = 5.39–3.89 eV for Li–Cs),[41] the charge in the M^+LC complexes remains mostly on the metal. There is a small but noticeable charge transfer from M to LC, which increases from Cs to Li (Δq_M = 87–127 me) with the strength of the interaction (Table 4, Fig. S4 in ESI†). The charge transfer to O4 is stronger than to N5 (Δq_{O4} = 136–156 me, Δq_{N5} = 83–160 me), in line with the shorter bonds. There is also minor charge rearrangement on the remote C═O2 group (Δq_{O2} = 45–63 me). Metalation at O4 has a strong impact on the C═O4 bond length and the frequency of the corresponding strongly IR active stretch mode. The stronger the interaction, the larger the elongation of the C═O4 bond and the lower

Table 3 Bond lengths and angles (Å, degrees) and C═O stretch frequencies (cm^{-1}) of $M^{q+}LC_n(O4)$ and $M^{q+}LC_n(O2)$ calculated at the B3LYP/cc-pVDZ level. Also listed are the ionic radii of M^{q+}

	R_M [a]	R_{MO4}	R_{MN5}	R_{CO2}	R_{CO4}	α_{N5MO4}	α_{MO4C4}	ν_{CO4} [b]	ν_{CO2} [b]
LC	—			1.2144	1.2121			1746 (383)	1799 (927)
$H^+LC(N5)$	0.37	2.344	1.029	1.2023	1.2162	102.2	82.8	1737 (363)	1797 (814)
$H^+LC(O4+)$	0.37	0.988	2.188	1.1998	1.3010	113.5	107.0	1633 (351)	1814 (1032)
$Li^+LC(O4)$	0.76	1.868	2.064	1.2032	1.2467	88.5	109.5	1651 (519)	1799 (939)
$Na^+LC(O4)$	1.02	2.201	2.437	1.2048	1.2391	74.3	116.0	1665 (517)	1795 (947)
$K^+LC(O4)$	1.38	2.519	2.872	1.2057	1.2369	62.6	123.8	1678 (575)	1808 (956)
$Rb^+LC(O4)$	1.52	2.651	3.048	1.2061	1.2354	58.9	126.4	1684 (592)	1807 (961)
$Cs^+LC(O4)$	1.67	2.814	3.297	1.2065	1.2348	54.4	130.3	1683 (637)	1806 (968)
$Ag^+LC(O4)$	1.15	2.322	2.304	1.2036	1.2405	75.3	110.9	1650 (523)	1798 (947)
$Mg^{2+}LC(O4)$	0.72	1.920	2.058	1.1936	1.2838	87.9	109.1	1609 (560)	1830 (877)
$Mg^{2+}LC_2(O4)$	0.72	1.991	2.164	1.1984	1.2639	82.1	113.0	1629 (16)	1815 (440)
								1622 (1369)	1814 (1411)

	R_M [a]	R_{MO2}	R_{CO2}	R_{CO4}	α_{N3C2O2}	α_{MO2C2}	ν_{CO4} [b]	ν_{CO2} [b]
$H^+LC(O2-)$	0.37	0.973	1.3152	1.1971	124.0	113.6	1800 (410)	1647 (571)
$Li^+LC(O2)$	0.76	1.728	1.2635	1.2033	121.5	177.8	1777 (376)	1649 (1632)
$Na^+LC(O2)$	1.02	2.087	1.2547	1.2049	121.8	177.9	1771 (368)	1660 (1587)
$K^+LC(O2)$	1.38	2.428	1.2509	1.2056	122.0	177.6	1784 (366)	1670 (1713)
$Rb^+LC(O2)$	1.52	2.566	1.2482	1.2060	122.0	177.4	1783 (364)	1677 (1784)
$Cs^+LC(O2)$	1.67	2.749	1.2472	1.2063	122.1	177.4	1782 (364)	1674 (1883)
$Ag^+LC(O2)$ [c]	1.15	2.120	1.2658	1.2028	119.1	141.0	1794 (369)	1642 (1607)
$Mg^{2+}LC(O2)$	0.72	1.824	1.2892	1.1952	121.7	163.2	1804 (322)	1585 (95)
$Mg^{2+}LC_2(O2)$	0.72	1.824	1.2962	1.1983	120.9	175.3	1795 (110)	1627 (1)
							1795 (718)	1597 (2646)

[a] Ref. 47. The values are effective ionic radii for the coordination number CN = 6. For H^+, the covalent radius is taken as half of the equilibrium separation of H_2 (0.74 Å). [b] IR intensities (km mol^{-1}) are listed in parentheses. [c] O2 is the O2− structure following the notation in ref. 18 (Fig. 4).

Table 4 NBO charge distribution (in *e*) of $M^{q+}LC_n(O4)$ and $M^{q+}LC_n(O2)$ calculated at the B3LYP/cc-pVDZ level[a]

	q_M	Δq_{O4}	Δq_{N5}	Δq_{O2}
$H^+LC(O4)$	0.522	−0.486	−0.367	−0.632
$Li^+LC(O4)$	0.873	−0.156	−0.160	0.063
$Na^+LC(O4)$	0.912	−0.140	−0.132	0.054
$K^+LC(O4)$	0.915	−0.141	−0.106	0.049
$Rb^+LC(O4)$	0.923	−0.135	−0.097	0.047
$Cs^+LC(O4)$	0.913	−0.136	−0.083	0.045
$Ag^+LC(O4)$	0.798	−0.102	−0.149	0.061
$Mg^{2+}LC(O4)$	1.707	−0.257	−0.305	0.122
$Mg^{2+}LC_2(O4)$	1.496	−0.187	−0.200	0.092

	q_M	Δq_{O2}	Δq_{N5}	Δq_{O4}
$H^+LC(O2)$	0.532	−0.541	−0.436	−0.606
$Li^+LC(O2)$	0.932	−0.269	0.016	0.048
$Na^+LC(O2)$	0.956	−0.227	0.015	0.039
$K^+LC(O2)$	0.955	−0.208	0.014	0.036
$Rb^+LC(O2)$	0.957	−0.195	0.013	0.034
$Cs^+LC(O2)$	0.956	−0.187	0.013	0.032
$Ag^+LC(O2)$ [b]	0.863	−0.191	0.018	0.054
$Mg^{2+}LC(O2)$	1.440	−0.337	0.048	0.099
$Mg^{2+}LC_2(O2)$	1.699	−0.340	0.024	0.073

[a] Δq are the charge differences with respect to neutral LC (available in Fig. S8 in ESI). All other atomic charges are less affected by metalation. [b] O2 is the O2− structure following the notation in ref. 18 (Fig. 4).

ν_{CO4} (ΔR_{CO4} = 23–35 mÅ, $-\Delta\nu_{CO4}$ = 63–95 cm^{-1}). Interestingly, also the free C═O2 bond is affected by conjugation through the pyrimidine ring, with a contraction of $-\Delta R_{CO2}$ = 8–11 mÅ and corresponding blueshifts of $\Delta\nu_{CO2}$ = 0–7 cm^{-1}.

The planar O2 isomer (C_s), in which M^+ binds in a linear configuration (deviation from linearity is $<1^\circ$) to the C═O2 carbonyl group of LC, is a less stable isomer of M^+LC (Fig. 1, Table 2). The energy difference of $M^+LC(O2)$ to the $M^+LC(O4)$ isomer is smallest for Cs with 32 kJ mol^{-1} and increases to 72 kJ mol^{-1} for Li. The free energy difference shows the same trend (29–68 kJ mol^{-1}). Despite the weaker total interaction, the M–O2 bonds in the O2 isomers (R_{MO2} = 1.73–2.75 Å) are shorter than the M–O4 bonds in the O4 isomers (R_{MO4} = 1.87–2.81 Å). This observation indicates that the M–N5 interaction provides a substantial additional stabilization of $M^+LC(O4)$. As a result, the total charge transfer from M^+ to LC is larger for the O4 isomer as compared to the O2 isomer (Δq_M = 87–127 *vs.* 44–68 me). As expected, metalation at O2 has a strong impact on the C═O2 bond length and the frequency of the corresponding strongly IR active stretch mode (ΔR_{CO2} = 33–49 mÅ, $-\Delta\nu_{CO2}$ = 125–150 cm^{-1}), and these changes are again larger than those of the C═O4 bond upon metalation in the O4 isomers of M^+LC. Similarly, also the free C═O4 bond in $M^+LC(O2)$ is affected by conjugation through the pyrimidine ring, with a contraction of ΔR_{CO4} = 6–9 mÅ and corresponding blueshifts of $\Delta\nu_{CO4}$ = 31–36 cm^{-1}.

The calculated spectrum of LC in Fig. 3 shows two free C═O stretch modes near 1800 cm^{-1}. Formation of M^+LC complexes with the M^+ ion attached to one of the carbonylic O atoms substantially reduces the corresponding C═O stretch frequency, as a result of partial electron transfer from the C═O group to the nearby metal ion. At the same time, the remaining free C═O stretch frequency increases by a smaller amount. Comparison of the measured M^+LC spectra with that predicted for bare LC reveals substantial red- and blueshifts for the two C═O stretch modes, indicating that the M^+ ion must bind to one of the two available C═O groups. This spectral result immediately excludes an assignment to any π

complex and also the N10-bonded σ-complex of M^+LC, in line with the thermochemical data (Fig. S3 in ESI† for Li^+LC). As several of the C═O stretch bands A and B exhibit shoulders or even resolved splittings, it is obvious that both possible CO-bonded σ-complexes are present in the ion cloud (at least for K–Cs), namely the most stable O4 and O2 isomers.

By comparison with the calculations, bands A and B are then readily assigned to the two C═O stretch modes of the C═O4 and C═O2 groups of LC in M^+LC in the most stable O4 and O2 isomers. Band A is assigned to the free C═O stretch (ν_{CO}^{f}), *i.e.* ν_{CO2} for the O4 isomer and ν_{CO4} for the O2 isomer. Accordingly, band B is assigned to the bound C═O stretch (ν_{CO}^{b}), *i.e.* ν_{CO4} of the O4 isomer and ν_{CO2} of the O2 isomer. Band C is identified as one of the ring skeleton C–N/C–C stretch vibrations (ν_{CN}). In general, the redshift of the bound C═O stretch and the blueshift of the free C═O stretch increase with the strength of the interaction. As larger alkali ions have weaker bonds, the shifts increase with decreasing size of the alkali ions. Apparently, the calculations slightly overestimate the separation between the two C═O stretch modes.[21]

From the comparison between the calculated and the experimental spectra in Fig. 3, the splittings and shoulders of bands A and B clearly demonstrate the presence of both the more stable O4 and the less stable O2 isomer. The roughly constant splitting of band A (free C═O stretch) is clearly resolved for the larger alkali ions K–Cs, and the calculations assign the higher-frequency component to ν_{CO2} of the O4 isomer and the lower-frequency component to ν_{CO4} of the O2 isomer. As the splitting is not resolved for Li^+LC and Na^+LC, it is unclear whether both isomers are present for these complexes. As the energy difference between the two isomers increases with decreasing size of the alkali ion, it is expected that the population of the less stable O2 isomers becomes smaller. On the other hand, as the binding energies increase for the smaller ions, the broadening effects of the IRMPD process may be more severe and prevent the resolution of the doublet arising from the two isomers.

Although the IRMPD spectra of M^+LC with M = K–Cs clearly show the presence of both the O4 and O2 isomers, it is difficult to quantify their population due to nonlinearities in the IRMPD cross sections and the (partly) overlapping bands. At first glance, the substantial abundance of the less stable O2 isomer is somewhat surprising, because its calculated relative free energy differs from the O4 isomer by 29 kJ mol^{-1} for Cs and increases to 68 kJ mol^{-1} for Li. Thus, at thermal equilibrium the population of the M^+LC(O2) isomer is not expected at room temperature and must therefore arise from the ESI process. It is conceivable, that the observed O2/O4 isomer ratio may reflect the one in solution, where solvation energies with surrounding solvent molecules are large for the M^+ cations and thus likely reduce the relative energy difference of the O4 and O2 isomers as compared to the gas phase.

For completeness, we also consider metal ion complexes of a low-energy tautomer of LC, denoted iso-LC, in which the proton from N1 is moved to N10 (Fig. S7 in ESI†). Although iso-LC is calculated to be less stable than LC by ΔE = 53.5 and ΔG = 53.0 kJ mol^{-1}, it may be populated in solution by solvent stabilization effects and generate M^+iso-LC complexes in the ESI source. Test calculations for Li^+iso-LC complexes yield quite stable planar O4 and O2 isomers, with binding free energies of 269 and 262 kJ mol^{-1}, which are indeed comparable to those of the corresponding Li^+LC isomers (272 and 204 kJ mol^{-1}). However, the IR spectra predicted for the O4 and O2 isomers of Li^+iso-LC are quite different from those of the corresponding isomers of Li^+LC and also the IRMPD spectrum measured for Li^+LC (Fig. S7 in ESI†). Hence, we can safely exclude the presence of iso-LC complexes in the sampled Li^+LC ion population and assume the same scenario for the other $M^{q+}LC_n$ complexes.

It is instructive to compare the properties of the M^+LC complexes with those of the isovalent H^+LC ion.[18] As the proton is very small, it can actually bind either to N5 or to O4, and both isomers are separated by appreciable proton transfer barriers of 73 and 51 kJ mol^{-1}. In the most stable H^+LC structure, the excess proton forms a covalent bond to the N5 atom, with a proton affinity of 934 kJ mol^{-1}. The O4 isomer is slightly less stable (by ~20 kJ mol^{-1}) and has a similar structure as the most stable M^+LC(O4) isomers, although the bond to the proton is much stronger (914 kJ mol^{-1}). As the alkali ions have a much larger ionic radius, they form weaker bonds and have only a single minimum in this area of the potential, with the bond to O4 being slightly stronger than that to N5 (in contrast to H^+). As for H^+LC only the more stable N5 isomer is detected, the IRMPD spectrum of H^+LC is qualitatively different from those of M^+LC (Fig. 2 and 3). Significantly, the H^+LC spectrum is dominated by two intense free C═O stretch bands and lack a bound C═O stretch transition. Many of the energetic, structural, and vibrational parameters predicted for the O4 isomer of H^+LC are obtained by extrapolating the properties of M^+LC(O4) as a function of the inverse ionic/covalent radius (Fig. S4–S6 in ESI†).

3.2 Ag^+LC

Similar to all flavins, LC does not show any special affinity for common d metal ions in aqueous solution.[11] The electronic configuration of the closed-shell Ag^+ coinage metal ion is $d^{10}s^0$ and thus similar to the alkali ions discussed above. However, while alkali ions bind to LC *via* electrostatic and induction forces, there may be additional orbital interactions with Ag^+ arising from $d^{10-x}s^x$ hybridization, which leads to enhanced covalent contributions to the Ag^+–LC interaction.[42] Such orbital interactions have previously been analysed for Ag^+ binding to pyridine, phenol, and polycyclic aromatic hydrocarbons *via* IR(M)PD spectra and quantum chemical calculations.[29,30,32] As the calculated ionization energy of LC (IE = 7.99 eV) is slightly higher than that of Ag (IE = 7.58 eV),[41] the charge in $[AgLC]^+$ complexes is mostly localized on the metal atom, justifying the Ag^+LC notation. Because of the similar IE values of Ag and LC, charge transfer interaction involving the π HOMO of LC may stabilize π complexes of Ag^+LC relative to the σ complexes. Therefore, we again considered π complexes in more detail for Ag^+LC.

The calculations for Ag^+LC reveal that the σ-bonded planar O4 structure with chelate bonding to O4 and N5 is the most stable isomer with G = 260 kJ mol^{-1}. Interestingly, there is a

second O4-bound minimum, in which the Ag ion binds away from N5, denoted $Ag^+LC(O4-)$. This isomer has a considerably lower binding free energy of 183 kJ mol^{-1} because it lacks the attractive Ag^+–N5 interaction. No such O4− isomers are found for M^+LC with alkali ions, for which such geometries optimize towards the $M^+LC(O4)$ global minima. Apparently, Ag^+ likes to form bent C═O–Ag configurations (similar to H^+), whereas alkali ions prefer a linear approach to the C═O groups (in absence of the M^+–N5 attraction). The same observation holds for the two O2 isomers of Ag^+LC, namely $Ag^+LC(O2-)$ and $Ag^+LC(O2+)$, in which Ag^+ binds to C═O2 group in a bent configuration, whereas alkali metals prefer (nearly) linear bonds. The preference for forming bent C═O–Ag bonds may be taken as first indication of covalent contributions of Ag bonding to LC (*vide infra*). The three σ-bonded Ag^+LC isomers O4−, O2+, and O2− have roughly the same binding free energies (174–183 kJ mol^{-1}). The search for π complexes of Ag^+LC yielded a stable minimum, in which Ag forms a covalent bond to the C9 atom of the benzene ring, denoted $Ag^+LC(I)$. However, this isomer has a significantly lower binding energy (G = 133 kJ mol^{-1}). Such structures have previously been predicted and observed for Ag^+ complexes with phenol[32] and polycyclic aromatic hydrocarbon molecules, including naphthalene and azulene,[29] with binding energies in the range 150–200 kJ mol^{-1}. The IR spectra and structures calculated for all isomers are compared in Fig. 4, and the relevant structural, energetic and vibrational properties of the O4 and O2+ isomers are summarized in Tables 2–4. While the O4 and O4− spectra are clearly different due to the additional Ag^+–N5 interaction in the former isomer, the spectra of the O2± spectra are essentially the same. The spectrum of the $Ag^+LC(I)$ isomer is again different because this isomer has two free C═O bonds and no Ag^+–O interaction.

Closer inspection of Fig. 4 reveals a good match between the IRMPD spectrum of Ag^+LC with the IR spectrum predicted for the most stable isomer, $Ag^+LC(O4)$, in particular with respect to the positions and relative intensities of bands A–C. Clearly, other isomers provide at most only a minor contribution. The low-frequency shoulder of band B at 1640 cm^{-1} marked by an asterisk may indicate the minor presence of the O4− and/or O2± isomers.

Interestingly, the IRMPD spectrum of Ag^+LC is strikingly similar to the one measured for Li^+LC (Fig. 4), and this similarity is fully reproduced by the calculated spectra of their most stable isomers, $Ag^+LC(O4)$ and $Li^+LC(O4)$, as shown in Fig. S8 in ESI.† Such similarities have previously been reported for the IR spectra of Ag^+ and Li^+ complexes with other bioorganic molecules, such as arginine and tryptophan.[24,25] Indeed, the calculated binding free energies are quite similar for the O4 complexes of Li^+LC and Ag^+LC (272 and 262 kJ mol^{-1}), which explains the similar impact of the metal ion complexation on the C═O4 bond properties. However, the metal ligand bond distances are quite different in both complexes. As Ag^+ has a much larger ionic radius than Li^+ (1.15 and 0.76 Å), the M^+–O4 and M^+–N5 bonds are much longer in $Ag^+LC(O4)$ as compared to $Li^+LC(O4)$, R_{MO4} = 2.32 and 1.87 Å and R_{MN5} = 2.30 and 2.06 Å, respectively. From this difference in bond distances and the similar interaction energies, we conclude that the type of interaction in $Ag^+LC(O4)$ is different from that in $Li^+LC(O4)$. While bonding in the case of alkali ions to LC is dominated by electrostatic and inductive forces, as supported by the monotonic relation between the inverse metal ion radius and the binding energy (Fig. 5) and other geometric parameters (Fig. S4–S6 in ESI†), the Ag^+ interaction with LC has a substantial contribution of covalent bonding. The first indication

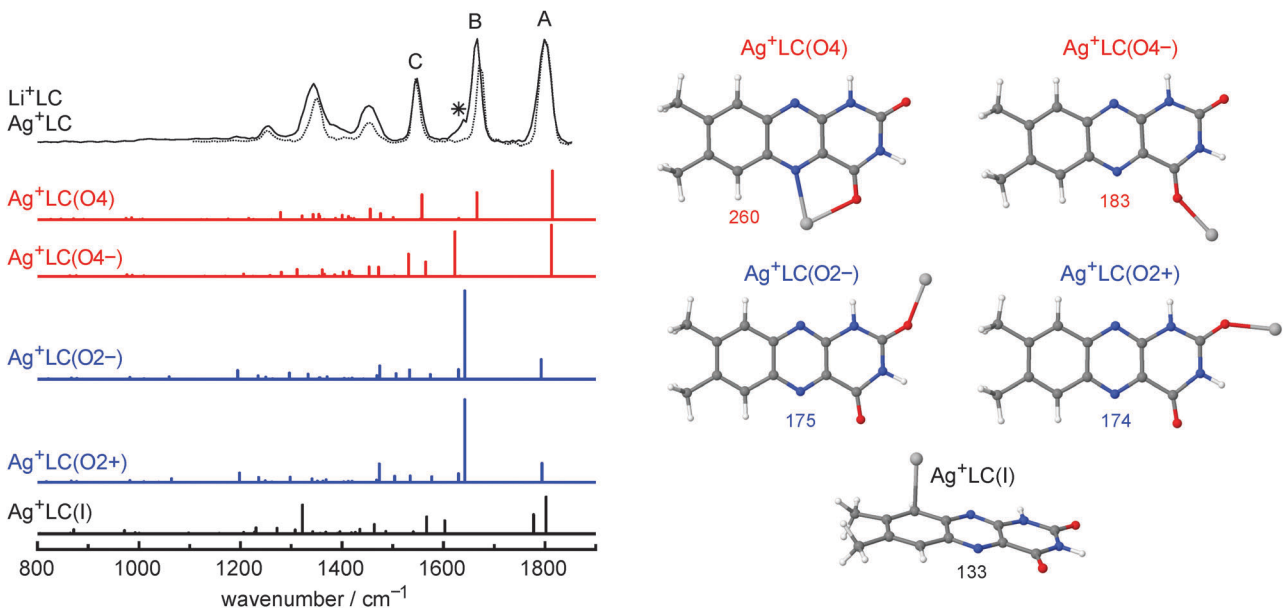

Fig. 4 IRMPD spectra of Ag^+LC (solid line) and Li^+LC (dotted line) compared to linear IR stick absorption spectra of $Ag^+LC(O4)$, $Ag^+LC(O4-)$, $Ag^+LC(O2-)$, $Ag^+LC(O2+)$, and $Ag^+LC(I)$ calculated at the B3LYP/cc-pVDZ level. The structures of the Ag^+LC isomers and their binding free energies (kJ mol^{-1}) are also shown.

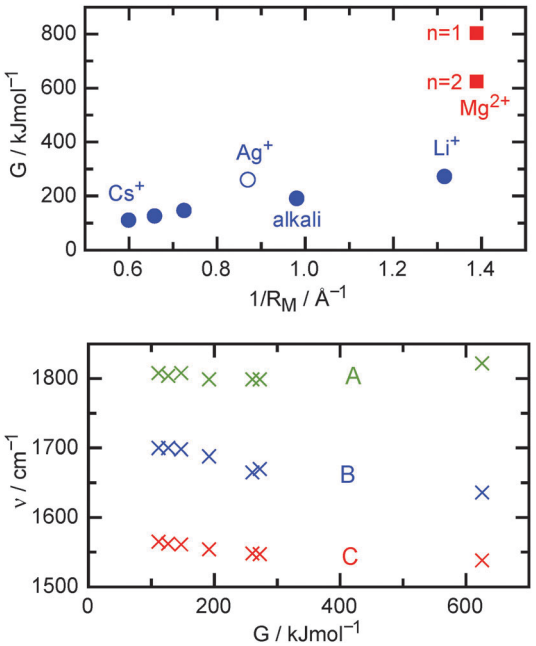

Fig. 5 (top) Plot of free energies of the O4 isomers of M^+LC (M = Li–Cs, filled blue circles), Ag^+LC (open blue circle), and $Mg^{2+}LC_n$ (n = 1 and 2, filled red squares) as a function of the inverse ionic radius of the metal ion. (bottom) Positions of the bands A–C in the IRMPD spectra of $M^{q+}LC_n$ as a function of the free energies of the O4 isomers.

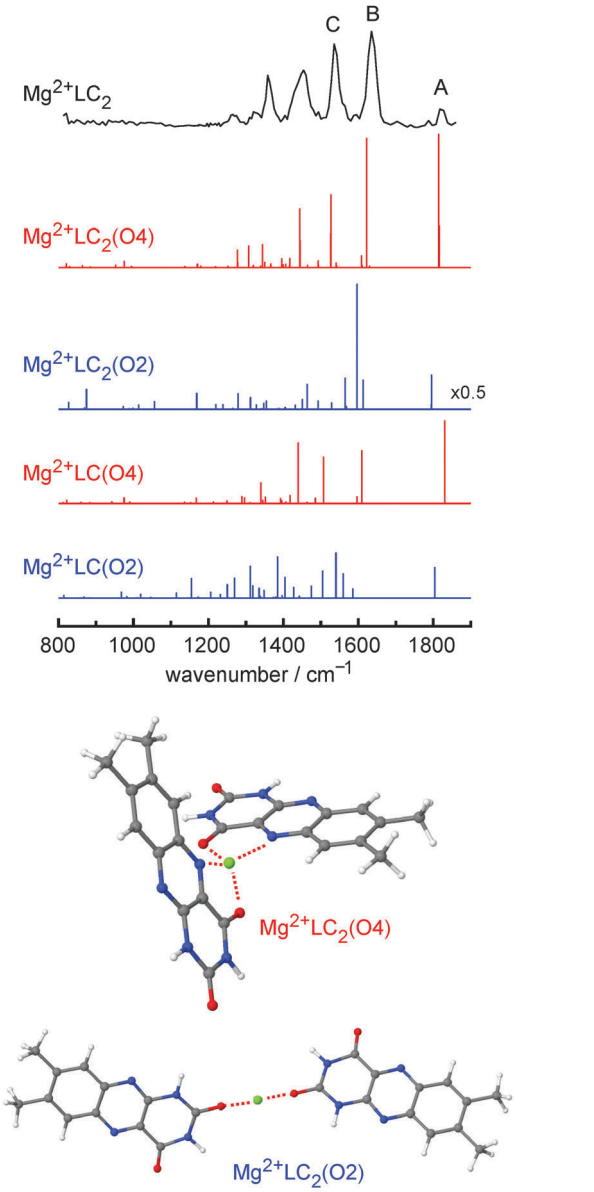

Fig. 6 IRMPD spectrum of $Mg^{2+}LC_2$ compared to linear IR stick absorption spectra of $Mg^{2+}LC_n$(O4) and $Mg^{2+}LC_n$(O2) with n = 1 and 2 calculated at the B3LYP/cc-pVDZ level. The intensity of band A in the IRMPD spectrum is reduced due to low laser intensity (Fig. S1 in ESI†).

for this conclusion has come from the observation that alkali ions prefer linear bonding to the C═O groups (in the absence of the M^+–N5 interaction), while Ag^+ prefers a bent C═O–Ag^+ configuration. The latter is similar to C═O–H^+, where the proton also forms a largely covalent bond to C═O.[18] Moreover, the charge transfer from Ag^+ to LC is much larger than for Li^+ (202 and 127 me), again supporting the scenario of additional covalent contributions. Closer inspection of the M^+–O4 and M^+–N5 bond distances in M^+LC complexes as a function of the inverse ionic radius show that Ag^+ has a particularly enhanced affinity to N5, while the distances to O4 are regular. Apparently, Ag^+ exhibits an enhanced affinity to the N5 lone pair, and such enhanced bonding of Ag^+ to N as compared to O has been reported previously.[43,44]

In Fig. 5 the free energies of the O4 isomers of the considered M^+LC dimers are plotted as a function of the inverse ionic radius of M^+. For the alkali ions, the dependence is monotonic and roughly linear as expected for mainly Coulombic interactions (electrostatics and induction). Clearly, Ag^+LC deviates from the linear trend due to the additional covalent contribution discussed above. On the other hand, the positions of the bands A–C on the IRMPD spectra of M^+LC and Ag^+LC show a monotonic dependence as a function of the interaction free energy, indicating that the vibrational frequency shifts are a sensitive indicator of the bond strength for both the alkali ions and Ag^+.

3.3 $Mg^{2+}LC_2$

In an effort to explore the influence of a higher metal ion charge on the $M^{q+}LC$ interaction, we have chosen alkaline earth metal ions, M^{2+}. Unfortunately, the preparation of $M^{2+}LC$ dimers such as $Mg^{2+}LC$, $Ca^{2+}LC$, and $Ba^{2+}LC$ has not been successful under the employed ESI conditions. However, in the magnesium case, the mass spectrum reveals the production of $Mg^{2+}LC_2$ trimer complexes, which have been characterized by IRMPD and quantum chemical calculations (Fig. 6). Interestingly, the predominant IRMPD fragment channel of $Mg^{2+}LC_2$ does not correspond to the loss of intact LC ligands, like for the singly charged M^+LC complexes discussed above, but involves charge separation, leading to $[MgOH]^+LC$ and $[LC–OH]^+$ fragment ions. The resulting IRMPD spectrum of $Mg^{2+}LC_2$ in Fig. 2 is similar in appearance to the M^+LC dimer spectra. The major difference is a larger splitting in the two C═O stretch bands (A and B) resulting from the stronger interaction of the doubly charged ion.

Similar to the M^+LC dimers, π complexes of $Mg^{2+}LC$ are calculated to be substantially less stable than the σ complexes and are thus not considered further. This procedure is also justified by the IRMPD spectrum of $Mg^{2+}LC_2$, where the large splitting of the bands A and B indicates σ bonding of Mg to one of the C═O groups of each of the LC ligands. The relatively low interaction energy of 523 kJ mol^{-1} calculated for $Mg^{2+}LC(I)$ is similar to the one predicted for the π-bonded Mg^{2+}benzene complex (455 kJ mol^{-1}).[45] As for the singly charged ions, the O4 isomer of $Mg^{2+}LC$ is calculated to be more stable than the O2 isomer (G = 803 and 632 kJ mol^{-1}). The large energy difference between both isomers suggests that bonding to C═O4 is largely preferred over bonding to C═O2. In general, the structural, energetic, and vibrational trends discussed for the M^+LC dimers with the alkali ions in Section 3.1 apply also to the $Mg^{2+}LC(O4/O2)$ dimers, for which the effects are much more pronounced due to the much stronger bonding arising from the twofold positive charge (Tables 2–4, Fig. 5, Fig. S4–S6 in ESI†). Also, the charge transfer from Mg^{2+} to the LC ligands is much larger than for M^+LC (Δq_M = 293 and 560 me for the O4 and O2 isomers), although there is no direct correlation between binding energies and the charge transfer among the $Mg^{2+}LC(O4/O2)$ isomers. This may be due to different hybridisation schemes arising from linear and bifurcated bonding of Mg^{2+}. As the ionic radius of Mg^{2+} is similar to that of Li^+ (R_M = 0.72 and 0.76 Å), also their M–O and M–N bond lengths and bond angles are similar for both the O4 and O2 isomers due to the steep rise in the Pauli repulsion of the potential. However, the doubled charge in $Mg^{2+}LC$ leads to a substantially stronger interaction than in Li^+LC (G = 803 and 272 kJ mol^{-1}) and a correspondingly larger impact on the C═O bond properties, with larger changes in their bond lengths and stretching frequencies upon metal complexation. The IR spectra calculated for $Mg^{2+}LC(O4)$ and $Mg^{2+}LC(O2)$ are quite different in the fingerprint range (Fig. 6).

On the basis of the structures of the σ-bonded $Mg^{2+}LC$ dimers, we calculated selected $Mg^{2+}LC_2$ trimer structures, in which both LC ligands are separately binding to Mg^{2+} either *via* their C═O4 or their C═O2 groups, denoted $Mg^{2+}LC_2(O4)$ and $Mg^{2+}LC_2(O2)$, respectively (Fig. 6). In the more stable $Mg^{2+}LC_2(O4)$ complex, the Mg^{2+} ion is tetra-coordinated to the two N5 and O4 atoms of the two LC ligands in a pyramidal configuration, and the two planar LC units include an angle of 69°. Its total binding free energy of G = 1251 kJ mol^{-1} implies a bond energy of 625 kJ mol^{-1} per LC ligand, which is substantially smaller than the Mg^{2+}–LC bond energy of the $Mg^{2+}LC(O4)$ dimer, G = 803 kJ mol^{-1}. Such noncooperative effects are quite common for sequential solvation of charged ions,[46] and result from increasing charge delocalization and noncooperative induction forces. Indeed, the charge transfer from Mg^{2+} to the LC ligands is 293 and 504 me for $Mg^{2+}LC_n(O4)$ with n = 1 and 2, respectively. As a consequence of the weaker interaction in the n = 2 complex, the metal–ligand bond lengths are larger and the corresponding effects on the C═O bond properties (R_{CO}, ν_{CO}) correspondingly smaller. Nonetheless, the appearance of the IR spectra of $Mg^{2+}LC_n(O4)$ with n = 1 and 2 is quite similar (Fig. 6). In particular, no new intense bands appear upon complexation with the second LC ligand, indicating that the coupling between both LC ligands is rather weak.

In the less stable $Mg^{2+}LC_2(O2)$ isomer, the Mg^{2+} ion is twofold coordinated to the two O2 atoms of the two LC ligands in a linear arrangement, and the two planar LC units include an angle of 40°. The bond energy of G = 497 kJ mol^{-1} per LC ligand derived from the total binding free energy of 995 kJ mol^{-1} is again substantially smaller than the Mg^{2+}–LC(O2) bond energy, G = 632 kJ mol^{-1}, due to the noncooperativity. Similarly, the weaker interaction in the n = 2 complex leads to longer metal–ligand bonds lengths and smaller effects on the C═O bond properties (R_{CO}, ν_{CO}) as compared to n = 1. Interestingly, the IR spectrum of the n = 2 complex is quite different from that of the n = 1 complex, with respect to both the vibrational frequencies and the IR intensities.

Significantly, the IR spectra predicted for the $Mg^{2+}LC_2(O4)$ and $Mg^{2+}LC_2(O2)$ trimers are quite different, and only the spectrum of the more stable $Mg^{2+}LC_2(O4)$ complex compares favourably with the IRMPD spectrum (Fig. 6). The major discrepancy between measured and calculated spectra is the low relative intensity of band A in the IRMPD spectrum, which is attributed to the low IR laser power available in this frequency range (Fig. S1 in ESI†). In view of the IR multiple-photon absorption process, the applied linear power correction is insufficient for very low laser intensities near threshold of the IRMPD process. Although we cannot completely rule out minor contributions of the $Mg^{2+}LC_2(O2)$ isomer to the measured IRMPD spectrum, the latter is clearly dominated by the $Mg^{2+}LC_2(O4)$ isomer. Comparison of the M^+LC and $Mg^{2+}LC_2$ spectra shows distinctly the influence of the metal charge on their spectral properties (Fig. 2 and 5). While Li^+ and Mg^{2+} have nearly the same ionic radii (0.76 and 0.72 Å), the spectral shifts induced by the latter ion are much larger due to the doubled positive charge.

4. Concluding remarks

The interaction between metal ions and flavin molecules has been probed by IR spectroscopy and quantum chemical calculations of mass-selected $M^{q+}LC_n$ complexes generated in the gas phase. Significantly, these experiments are the first spectroscopic data of metal–flavin complexes in the gas phase and provide a first impression of the M^{q+}–flavin interaction free from interference effects arising from solvents and counter ions. The preferred binding site, strength and type of interaction have systematically been characterized for a variety of metal ions, namely alkali ions, Ag^+, and Mg^{2+}, to probe the dependence of the interaction on the charge, size, and type of the metal ion. For all $M^{q+}LC$ ions, the planar O4 isomer is identified as the most stable isomer both spectroscopically and theoretically. In this chelate configuration, the metal ion benefits from an interaction with the lone pairs of both the N5 and O4 atoms of LC. The O2 isomers lack the stabilization of the interaction with N5, leading to smaller binding energies. Nonetheless, this isomer is identified in the M^+LC spectra with M = K–Cs. The unexpected observation of these significantly less stable isomers is attributed to the ESI process from the

solution phase, which apparently generates a M^+LC isomer distribution far from the gas-phase thermodynamic equilibrium. For the alkali ions, all energetic, structural, electronic, and vibrational parameters of M^+LC scale monotonically and roughly linear with the inverse ionic radius of M^+. This behaviour is rationalized by the dominant contributions of Coulombic attractions (electrostatic and induction) to the attractive part of the interaction potential. In contrast, Ag^+LC deviates in many aspects from this trend, which is taken as strong indication of additional covalent contributions to the attraction, mainly *via* enhanced interaction with N5. This additional contribution implies that the Ag^+LC and Li^+LC interactions and IR spectra are similar, although the ionic radius of Ag^+ is substantially larger than that of Li^+. The interaction in $Mg^{2+}LC$ is again much stronger than that in the singly charged M^+LC complexes due to the doubled positive charge. Only the $Mg^{2+}LC_2$ trimer is observed under the current ESI conditions, and its IR spectrum is consistent with a structure, in which both LC ligands interact with the central metal ion core *via* their O4 and N5 lone pairs leading to a tetrahedral configuration for Mg^{2+}. In general, the vibrational shifts of the C=O stretch modes observed as strong transitions in the IRMPD spectra of all $M^{q+}LC_n$ complexes are a sensitive indicator of the metal binding site and the interaction strength. Complexation of LC with the metal cations is accompanied by electron transfer from the nonbonding lone pairs of N5 and O4 to the M^{q+}. As such, the charge transfer is mostly localized on the n orbitals of LC, whereas the electronic structure of the aromatic π electron system is less affected. Consequently, electronic $\pi \rightarrow \pi^*$ transitions may be less affected by metal complexation, whereas the respective $n \rightarrow \pi^*$ transitions may show large changes in their position, coupling, and lifetime. In the future, we will explore the optical spectra of these $M^{q+}LC_n$ complexes in order to probe the effects of metal complexation on the electronic structure of the LC chromophore in these fundamental metal–flavin hybrid complexes.

Acknowledgements

This work was supported by Technische Universität Berlin and Deutsche Forschungsgemeinschaft (DO 729/6). The research leading to these results has received funding from the European Community's Seventh Framework Program (FP7/2007-2013) under grant agreement no. 226716. This work is part of the research program of FOM, which is financially supported by the Nederlandse Organisatie voor Wetenschappelijk Onderzoek (NWO). We gratefully acknowledge the excellent assistance by the FELIX staff (B. Redlich *et al.*). We thank Sophie Seidenbecher and Judith Langer for assistance in the initial experimental and computational data acquisition.

References

1 E. Silva and A. M. Edwards, *Flavins*, The Royal Society of Chemistry, Cambridge, 2006.
2 P. F. Heelis, *Chem. Soc. Rev.*, 1982, **11**, 15–39.
3 A. Losi, *Photochem. Photobiol.*, 2007, **83**, 1283–1300.
4 A. Losi and W. Gartner, *Photochem. Photobiol.*, 2011, **87**, 491–510.
5 T. E. Swartz, T. S. Tseng, M. A. Frederickson, G. Paris, D. J. Comerci, G. Rajashekara, J. G. Kim, M. B. Mudgett, G. A. Splitter, R. A. Ugalde, F. A. Goldbaum, W. R. Briggs and R. A. Bogomolni, *Science*, 2007, **317**, 1090–1093.
6 V. Massey, *Biochem. Soc. Trans.*, 2000, **28**, 283–296.
7 M. Sugiyama, *Environ. Health Perspect.*, 1991, **92**, 63–70.
8 W. J. Rutter, *Acta Chem. Scand.*, 1958, **12**, 438–446.
9 D. Coursolle, D. B. Baron, D. R. Bond and J. A. Gralnick, *J. Bacteriol.*, 2010, **192**, 467–474.
10 M. Benecky, T. Y. Yu, K. L. Watters and J. T. McFarland, *Biochim. Biophys. Acta*, 1980, **626**, 197–207.
11 The Structure and Reactivity of Flavin-Metal Complexes, in *Inorganic Biochemistry*, ed. G. L. Eichhorn, 1973, vol. 2.
12 J. Lauterwein, P. Hemmerich and J. M. Lhoste, *Inorg. Chem.*, 1975, **14**, 2152–2161.
13 J. Lauterwein, P. Hemmerich and J. M. Lhoste, *Inorg. Chem.*, 1975, **14**, 2161–2168.
14 J. Lauterwein, P. Hemmerich and J. M. Lhoste, *Zeitschrift Für Naturforschung Part B-Chemie Biochemie Biophysik Biologie Und Verwandten Gebiete*, 1972, **B27**, 1047.
15 F. Müller, P. Hemmerich and A. Ehrenberg, *Eur. J. Biochem.*, 1968, **5**, 158.
16 J. Hasegawa, S. Bureekaew and H. Nakatsuji, *J. Photochem. Photobiol., A*, 2007, **189**, 205–210.
17 T. L. Zhang, K. Papson, R. Ochran and D. P. Ridge, *J. Phys. Chem. A*, 2013, **117**, 11136–11141.
18 J. Langer, A. Günther, S. Seidenbecher, G. Berden, J. Oomens and O. Dopfer, *ChemPhysChem*, 2014, DOI: 10.1002/cphc.201402146.
19 L. Guyon, T. Tabarin, B. Thuillier, R. Antoine, M. Broyer, V. Boutou, J. P. Wolf and P. Dugourd, *J. Chem. Phys.*, 2008, **128**, 075103.
20 A. Vdovin, A. Slenczka and B. Dick, *Chem. Phys.*, 2013, **422**, 195–203.
21 R. C. Dunbar, D. T. Moore and J. Oomens, *J. Phys. Chem. A*, 2006, **110**, 8316–8326.
22 L. MacAleese and P. Maitre, *Mass Spectrom. Rev.*, 2007, **26**, 583–605.
23 N. C. Polfer, J. Oomens, D. T. Moore, G. von Helden, G. Meijer and R. C. Dunbar, *J. Am. Chem. Soc.*, 2006, **128**, 517–525.
24 N. C. Polfer, J. Oomens and R. C. Dunbar, *Phys. Chem. Chem. Phys.*, 2006, **8**, 2744–2751.
25 M. W. Forbes, M. F. Bush, N. C. Polfer, J. Oomens, R. C. Dunbar, E. R. Williams and R. A. Jockusch, *J. Phys. Chem. A*, 2007, **111**, 11759–11770.
26 M. K. Drayß, P. B. Armentrout, J. Oomens and M. Schaefer, *Int. J. Mass Spectrom.*, 2010, **297**, 18–27.
27 R. C. Dunbar, J. D. Steill and J. Oomens, *J. Am. Chem. Soc.*, 2011, **133**, 1212–1215.
28 R. C. Dunbar, N. C. Polfer, G. Berden and J. Oomens, *Int. J. Mass Spectrom.*, 2012, **330**, 71–77.

29 M. Savoca, T. Wende, L. Jiang, J. Langer, G. Meijer, O. Dopfer and K. R. Asmis, *J. Phys. Chem. Lett.*, 2011, **2**, 2052–2056.
30 S. Chakraborty and O. Dopfer, *ChemPhysChem*, 2011, **12**, 1999–2008.
31 A. Lagutschenkov, A. Springer, U. J. Lorenz, P. Maitre and O. Dopfer, *J. Phys. Chem. A*, 2010, **114**, 2073–2079.
32 A. Lagutschenkov, R. K. Sinha, P. Maitre and O. Dopfer, *J. Phys. Chem. A*, 2010, **114**, 11053–11059.
33 A. Lagutschenkov, U. J. Lorenz and O. Dopfer, *Int. J. Mass Spectrom.*, 2011, **308**, 316–329.
34 D. Oepts, A. F. G. van der Meer and P. W. van Amersfoort, *Infrared Phys. Technol.*, 1995, **36**, 297–308.
35 J. J. Valle, J. R. Eyler, J. Oomens, D. T. Moore, A. F. G. van der Meer, G. von Helden, G. Meijer, C. L. Hendrickson, A. G. Marshall and G. T. Blakney, *Rev. Sci. Instrum.*, 2005, **76**, 023103.
36 J. Oomens, B. G. Sartakov, G. Meijer and G. von Helden, *Int. J. Mass Spectrom.*, 2006, **254**, 1–19.
37 M. J. Frisch, G. W. Trucks, H. B. Schlegel, G. E. Scuseria, M. A. Robb, J. R. Cheeseman, G. Scalmani, V. Barone, B. Mennucci, G. A. Petersson, H. Nakatsuji, M. Caricato, X. Li, H. P. Hratchian, A. F. Izmaylov, J. Bloino, G. Zheng, J. L. Sonnenberg, M. Hada, M. Ehara, K. Toyota, R. Fukuda, J. Hasegawa, M. Ishida, T. Nakajima, Y. Honda, O. Kitao, H. Nakai, T. Vreven, J. A. Montgomery Jr., J. E. Peralta, F. Ogliaro, M. Bearpark, J. J. Heyd, E. Brothers, K. N. Kudin, V. N. Staroverov, R. Kobayashi, J. Normand, K. Raghavachari, A. Rendell, J. C. Burant, S. S. Iyengar, J. Tomasi, M. Cossi, N. Rega, N. J. Millam, M. Klene, J. E. Knox, J. B. Cross, V. Bakken, C. Adamo, J. Jaramillo, R. Gomperts, R. E. Stratmann, O. Yazyev, A. J. Austin, R. Cammi, C. Pomelli, J. W. Ochterski, R. L. Martin, K. Morokuma, V. G. Zakrzewski, G. A. Voth, P. Salvador, J. J. Dannenberg, S. Dapprich, A. D. Daniels, Ö. Farkas, J. B. Foresman, J. V. Ortiz, J. Cioslowski and D. J. Fox, Gaussian, Inc., Wallingford, CT, 2009.
38 R. Ahlrichs, M. Bär, M. Häser, H. Horn and C. Kölmel, *Chem. Phys. Lett.*, 1989, **162**, 165–169.
39 P. J. Hay and W. R. Wadt, *J. Chem. Phys.*, 1985, **82**, 270–283.
40 J. Oomens, A. G. G. M. Tielens, B. G. Sartakov, G. von Helden and G. Meijer, *Astrophys. J.*, 2003, **591**, 968.
41 P. J. Linstrom and W. G. Mallard, *NIST Chemistry WebBook*, NIST Standards and Technology, Gaithersburg, MD, 2014, 20899, http://webbook.nist.gov.
42 B. Bellina, I. Compagnon, L. MacAleese, F. Chirot, J. Lemoine, P. Maitre, M. Broyer, R. Antoine, A. Kulesza, R. Mitric, V. Bonacic-Koutecky and P. Dugourd, *Phys. Chem. Chem. Phys.*, 2012, **14**, 11433–11440.
43 H. El Aribi, T. Shoeib, Y. Ling, C. F. Rodriquez, A. C. Hopkinson and K. W. M. Siu, *J. Phys. Chem. A*, 2002, **106**, 2908–2914.
44 H. El Aribi, C. F. Rodriquez, T. Shoeib, Y. Ling, A. C. Hopkinson and K. W. M. Siu, *J. Phys. Chem. A*, 2002, **106**, 8798–8805.
45 D. Vijay and G. N. Sastry, *Phys. Chem. Chem. Phys.*, 2008, **10**, 582–590.
46 R. G. Keesee and A. W. Castleman Jr., *J. Phys. Chem. Ref. Data*, 1986, **15**, 1011–1071.
47 R. D. Shannon, *Acta Crystallogr., Sect. A: Cryst. Phys., Diffr., Theor. Gen. Crystallogr.*, 1976, **32**, 751–767.